EXPERIMENTAL VALIDATION OF ZVS BOOST CONVERTER WITH RESONANT CIRCUIT FOR LOW POWER PHOTOVOLTAIC APPLICATIONS

SATARUPA BAL (109EE0252)

Department of Electrical Engineering
National Institute of Technology Rourkela

EXPERIMENTAL VALIDATION OF ZVS BOOST CONVERTER WITH RESONANT CIRCUIT FOR LOW POWER PHOTOVOLTAIC APPLICATIONS

A Thesis submitted in partial fulfillment of the requirements for the degree of

Bachelor of Technology in "Electrical Engineering "

By

SATARUPA BAL (109EE0252)

Under the guidance of

Prof. B. CHITTI BABU

Department of Electrical Engineering
National Institute of Technology
Rourkela-769008 (ODISHA)
May-2013

DEPARTMENT OF ELECTRICAL ENGINEERING

NATIONAL INSTITUTE OF TECHNOLOGY,

ROURKELA, ODISHA, INDIA-769008

CERTIFICATE

This is to certify that the thesis entitled "**Experimental Validation Of ZVS Boost Converter With Resonant Circuit For Low Power Photovoltaic Applications"**, submitted by **Satarupa Bal (Roll. No. 109EE0252)** in partial fulfilment of the requirements for the award of **Bachelor of Technology** in **Electrical Engineering** during session 2012-2013 at National Institute of Technology, Rourkela. A bonafide record of research work carried out by them under my supervision and guidance.

The candidates have fulfilled all the prescribed requirements.

The thesis which is based on candidates' own work, have not submitted elsewhere for a degree/diploma.

In my opinion, the thesis is of standard required for the award of a bachelor of technology degree in Electrical Engineering.

Place: Rourkela

Dr. B.ChittiBabu
Dept. of Electrical Engineering,
National institute of Technology,
Rourkela-769008, ODISHA.

ACKNOWLEDGEMENTS

I have been highly indebted in the preparation of this report to my supervisor, Prof. B. Chitti Babu, whose patience and kindness, as well as his academic experience, has been invaluable to me. I could not have asked for a better role model, inspirational, supportive, and patient guide. I could not be prouder of my academic roots and hope that I can in turn pass on the research values and the dreams that he has given to me.

The informal support and encouragement of many friends has been indispensable, and I would like particularly to acknowledge the contribution of all the students working under Prof. B. Chitti Babu.

I would not have contemplated this road if not for my parents, who instilled within me a love of creative pursuits, science and language, all of which finds a place in this report.

\

Satarupa Bal

B.Tech (Electrical Engineering)

Dedicated to

My Lovable Parents

ABSTRACT

This thesis presents mathematical analysis of the photovoltaic (PV) model along with the comprehensive analysis of a resonant circuit based soft switching boost converter for PV applications. The converter maintains a Zero Voltage Switching (ZVS) turn-on and turn-off of the main switch, and Zero Current Switching (ZCS) turn-on and ZVS turn-off of the auxiliary switch due to the resonant circuit incorporated in the same. Detailed operation of the converter, analysis of various modes, simulation as well as experimental results for the design has also been aptly presented. Switching and conduction losses across the switches and the diodes have been calculated and analysed, and some light has also been thrown on the design of inductor used in the practical implementation. The Perturbation and Observation (P&O) method has been used in order to track the Maximum Power Point (MPP) from the PV panel. This soft switching technique has been aimed to be used in telecom services where there is a necessity of 48 V regulated DC bus voltage. The systems are modelled and simulated in PSIM 64 bit version 9.0 environment and is experimentally validated in FPGA environment. Thus, the feasibility and the effectiveness of the system were also proven through theoretical analysis and experimental results.

CONTENTS

CHAPTER-3

SOFT SWITCHING DC-DC BOOST CONVERTER FOR PV APPLICATION

CHAPTER-4

RESULTS AND DISCUSSIONS

CHAPTER-5

CONCLUSION AND FUTURE WORK

LIST OF FIGURES

LIST OF TABLES

ABBREVIATIONS AND ACRONYMS

PV	-	Photo Voltaic
PVA	-	Photo Voltaic Array
SPV	-	Solar Photo Voltaic
MOSFET	-	Metal Oxide Semiconductor Field Effect Transistor
PWM	-	Pulse Width Modulation
EMI	-	Electro Magnetic Interference
ZVS	-	Zero Voltage Switching
ZCS	-	Zero Current Switching
MATLAB	-	MATrix LABoratory
MPPT	-	Maximum Power Point Tracking

CHAPTER 1

Introduction

1.1 MOTIVATION

Production of clean and green energy for modern power systems has become an increasingly burning area of research among the scientific community [1] and electrical energy from photovoltaic (PV) is currently regarded as the prerequisite sustainable resource, since it is free, abundant, clean and distributed over the earth. However, low efficiency is observed in photovoltaic systems accounting for the fact that it depends on parameters such as external temperature and irradiation [2].

In order to maximize the effectiveness of PV module, the PV power system also has to track the maximum possible power regardless of the unpredictable variations in the parameters and as they are generally integrated with specific control algorithms, in order to extract the maximum possible power, it becomes highly imperative that the MPP is achieved effectively. Some MPPT techniques like Perturbation and Observation, Current Compensation and Incremental Conductance methods have been proposed in [3-5] to track the MPP in an effective way. In this report, the Perturbation and Observation technique has been adopted for simplicity purposes.

1.2 PV ENERGY SYSTEM IN INDIAN SCENARIO

India imports more than 80% of its oil; hence it has a huge dependency on external sources for development. With depleting fossil reserves worldwide, there has been a threat to India's future energy security. Hence, the government of India is investing huge capital on development of alternative sources of energy such as solar, small hydroelectric, biogas and wind energy systems apart from the conventional nuclear and large hydroelectric systems [3].

The distribution of power generation from various sources according to the Ministry of New and Renewable Energy, Government of India as on 31.01.2013 is shown in Table 1.1.

TABLE 1.1: DISTRIBUTION OF POWER GENERATION IN INDIA FROM DIFFERENT SOURCES

Technology	Capacity Installed (GW)	Total Installed Capacity (%)
Thermal	167	52.02
Hydro	48	14.95
Renewable	53	16.51
Gas	49	15.26
Nuclear	4	2.14

From the year 2002 onwards, renewable grid capacity as a percentage of total capacity has increased by almost four times. In April 2002, renewable energy based power generation installed capacity was 3497 MW which was 3% of the total installed capacity in the country. India today stands among the top five countries of the world in terms of renewable energy capacity with an installed base of over 19000 MW of grid interactive renewable power which is around 11% of our total installed capacity.

Although the solar generation concept is popular among space applications, it is yet to get its importance in domestic applications owing high costs associated with generation of electricity from the solar arrays. However, the Ministry of New and Renewable Energy (MNRE), Government of India has taken several steps to highlight the generation of solar energy in Indian energy sector. India in particular should utilise the opportunity of higher solar insolation levels than most of the countries in the world to harness solar energy. The estimated potential of solar power that can be harnessed on the surface is 50MW/sq.km.

1.3 PV ENERGY SYSTEMS FOR PORTABLE APPLICATIONS

This energy generation system consists mostly of capacities below 100W. They have a huge range of applications ranging from powering calculators, educational toys, solar lamps, traffic signals, mobile chargers, etc. They are usually made up of poly crystalline material of solar cells due to their higher energy density over a small area and fits in the portable applications. However, this system is not highly commercialised due to battery technology required to store the power generated and high cost of poly crystalline silicon solar cells. They generally use lithium ion batteries [4] to store energy due to its high energy capacity and light in weight. These systems come handy when power is required on move and has a potential to revolutionise the current era of electronics with free power on move. The simple mobile charger based on PV energy system consists of a small solar module generally made of poly crystalline silicon, connected to the electrical load through a buck/boost converter for regulation of voltage at the load end [5]. This regulation is usually done using a feedback loop that senses the output voltage and tries to keep it at the desired output voltage required.

1.4 CONVERTER TOPOLOGY FOR PV SYSTEMS

DC-DC converters play an important role in interfacing the non-conventional energy sources like photovoltaic current to useful DC or AC form. It is therefore necessary that the interfacing converter should be highly efficient in transferring the power to ensure proper load management. The boost topology is the most popular topology for getting constant value

of high DC output [6] as it's simple power circuit leads to high efficiency and high reliability at low cost. In case of hard switching boost converters, due to overlapping of voltage and current waveforms during switching and the reverse recovery of the diode with each switching cycle, there is a high amount of switching loss associated with it.

In order to address these shortcomings, new power electronics circuits are designed based on resonant and soft-switching technologies [7]. In these cases, an increase in the efficiency of the system is accounted for, owing to non-overlapping of the voltage and current waveforms during switching. This results in decreased output ripple at higher values of frequencies [8]. Also, with an increase in frequency, it is possible to use smaller values of inductors and capacitors, which results in the reduction of the sizes of the components and thus increasing the power density [7]. However, the major challenge still remains as the design of the converter, especially when the constraints such as permissible stresses and conduction losses are stringent.

This thesis presents a soft switching technique that provides ZVS turn-on and turn-off for the main switch. The auxiliary switch ensures ZCS turn-on and ZVS turn-off process with the help of resonant circuit. An anti-parallel diode is added across the main switch so as to make the voltage zero across it before current starts building up and a capacitor is connected across the same to reduce the rate of rise of voltage across switch during turning-off process, thus ensuring ZVS. The auxiliary switch operates with ZCS using the resonance. This soft switching method is preferred over other methods because the resonant circuit implemented for soft switching performs dual operation. It not only ensures ZVS turn-off of the main switch and auxiliary switch but also the ZCS turn-on of the auxiliary switch. Hence, along with the conduction losses of the auxiliary switch, the switching loss is also decreased tremendously.

1.5 OVERVIEW OF PROPOSED WORKDONE

A resonant boost converter is seen to have improved efficiency of converter systems by reducing the switching losses, due to the implementation of ZVS and ZCS. It reduces the switching stress by forcing the current/voltage of a switch to zero prior to a switching transition. However, they introduce high current/voltage stresses in the switch. Hence to overcome this problem, ZVS scheme is implemented for the main switch, but the auxiliary switch still suffers from the capacitive turn-on loss. Reversal of inductor current is adopted and all the switches were turned-on with zero-current switching (ZCS) without causing any

over current or voltage stresses for the auxiliary switch. Also, the switching frequency is increased with reduction in components sizes as consequence of it [2]. However, these technique isn't feasible for wide load range and wide duty ratio range. The Zero Voltage transition (ZVT) and Zero Current Transition (ZCT) are able to solve the purpose [9-11]. Along with it, active-clamped current-fed-full-bridge converter is implemented for implementing ZVS condition over a wide range of load variation [12]. Various other soft switching techniques are also studied and discussed in the literature [13-14].

1.7 THESIS OBJECTIVES

The following objectives are hopefully to be achieved at the end of the project.

1) To study the mathematical modelling of PV array and observe its characteristics.
2) To study the proposed DC-DC Soft Switching Boost Converter and detailed analysis of the operation in various modes.
3) To validate the theoretical and simulation results experimentally in FPGA Environment.
4) To study the comparison of efficiency mainly in terms of switching and conduction between the conventional hard switching DC-DC boost converter and the proposed soft switching DC-DC boost converter.

1.8 ORGANISATION OF THE THESIS

The thesis is organised into six chapters including the chapter of introduction. Each chapter is different from the other and is described along with the necessary theory required to comprehend it.

Chapter 2 deals with the comparative study between various models of Photo-Voltaic (PV) array formulated exclusively using the data sheet parameters. The models used for comparative study in this paper includes ideal single diode model, the two diode model, the simplified single diode model and the improved single diode model. A typical 19.8W model is simulated and the output characteristics are observed. The comparative study has been made on basis of the MPP tracking, the RMSD from the experimental. Further, the resemblance of the P-V and I-V curves as obtained on the basis of experimental data has also been included in this study. On the basis of all these performance indices, the best model that can be used for simulation purposes has been selected. It is envisaged that the work can be very useful for professionals who require simple and accurate PV simulators for their design. All the systems here are modelled and simulated in MATLAB/Simulink environment.

Chapter 3 describes the design of a soft switching technique that provides ZVS turn-on and turn-off for the main switch. The auxiliary switch ensures ZCS turn-on and ZVS turn-off process with the help of resonant circuit. An anti-parallel diode is added across the main switch so as to make the voltage zero across it before current starts building up and a capacitor is connected across the same to reduce the rate of rise of voltage across switch during turning-off process, thus ensuring ZVS. The auxiliary switch operates with ZCS using the resonance. This soft switching method is preferred over other methods because the resonant circuit implemented for soft switching performs dual operation. It not only ensures ZVS turn-off of the main switch and auxiliary switch but also the ZCS turn-on of the auxiliary switch. Hence, along with the conduction losses of the auxiliary switch, the switching loss is also decreased tremendously. A detailed analysis of the mode by mode operation, design and simulation for the same, along with the calculation of the losses incurred in the converter has been done. The losses due to the inductors and the capacitors have not been taken into account and only the losses due to the switches and the diodes have been considered. Experimental results have also been shown for validation of the simulation results obtained. The procedure, used to design the main inductor has also been put forward here.

Chapter 4 presents the simulation results of the Soft Switching DC-DC Boost Converter carried out in PSIM. The results are validated experimentally in the Laboratory. The gate pulses of both the main and auxiliary MOSFET along with the voltage and current waveforms of the same are illustrated. The ZVS and ZCS is ensured in both the case. The PWM pulses are given to the control circuit through FPGA.

Chapter 5 concludes the work performed so far. The possible limitations in proceeding research towards this work are discussed. The future work that can be done in improving the current scenario is mentioned. The future potential along the lines of this work is also discussed.

CHAPTER 2

PV Array Modelling

2.1 INTRODUCTION

A solar cell is basically a p-n junction fabricated in a thin wafer of semiconductor. Being exposed to sunlight, photons with energy greater than the band-gap energy of the semiconductor create some electron-hole pairs proportional to the incident irradiation []. Generally, the I-V characteristics for a PV module composed of series connected cells based on single exponential model expressed as:

$$I_s = I_{ph} - I_o\left[e^{\left(\frac{q\left(V_{pv}+I_sR_sN_s\right)}{N_sKTA}\right)}-1\right]-\left(\frac{\left(V_{pv}+I_sR_sN_s\right)}{N_sR_{sh}}\right) \quad (2.1)$$

All the other parameters are mostly calculated through sets of non-linear equations.

2.2 MATHEMATICAL MODELLING OF PV ARRAY:

2.2.1 Ideal Single Diode Model (ISDM)

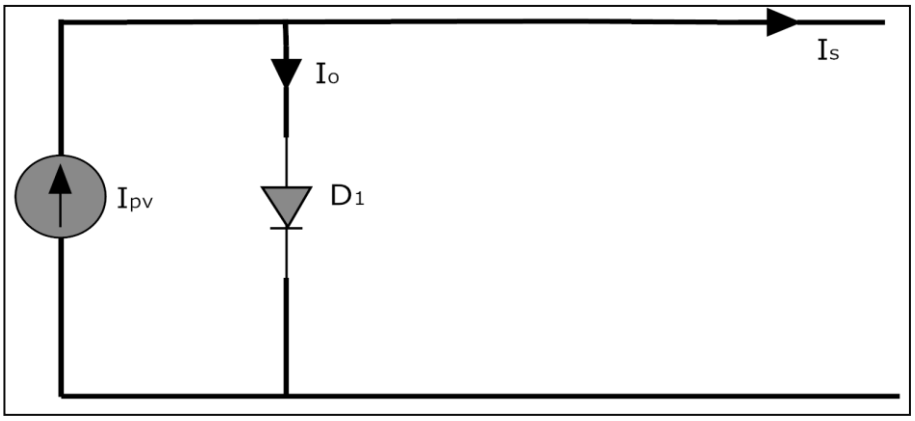

Fig.2.1PV cell modeled as ideal single diode circuit

The simplest equivalent circuit of a solar cell is a current source in parallel with a diode as illustrated in Fig.2.1. The output of the current source is directly proportional to the intensity of light falling on the cell i.e. photocurrent. Here the diode determines the I-V characteristics of the cell. The accuracy is increased by including temperature dependent diode saturation current (I_0), temperature dependent photocurrent (I_{ph}) and diode ideality factor (A) which lies between 1 and 2.

In an ideal cell R_s=R_{sh}=0, which is usually a common assumption. The equations are given as:

Module Photo-current (I_{ph}):

$$I_{ph} = \frac{[I_{scr} + K_i(T - 298)]G}{1000} \tag{2.2}$$

Module reverse saturation current (I_{rs}):

$$I_{rs} = \frac{I_{scr}}{e^{(qV_{oc}/N_sKAT)} - 1} \tag{2.3}$$

Module saturation current (I_0):

$$I_o = I_{rs}\left[\frac{T}{T_r}\right]^3 e^{\frac{qE_{go}}{BK(\frac{1}{T_r} - \frac{1}{T})}} \tag{2.4}$$

Output current (I_{pv}):

$$I_s = I_{ph} - I_o\left[e^{\left(\frac{qV_{pv}}{N_sKTA}\right)} - 1\right] \tag{2.5}$$

Here the ideality factor is assumed to be 1.6. However the output curve doesn't give accurate shape between the maximum power point the open-circuit voltage because of the exclusion of R_s. here the leakage current to the ground due to R_{sh} is also excluded.

2.2.2 Simplified Single Diode Model(SSDM)

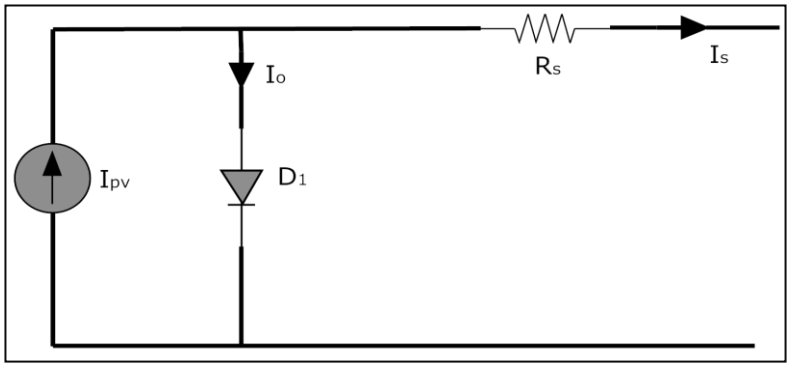

Fig 2.2 PV cell modelled as simplified single diode circuit

From the Fig.2.2, in the simplified single diode model the effect of R_{sh} is neglected for mathematical simplicity. The equation (2.1) reduces to

$$I_s = I_{ph} - I_o[e^{\frac{q(V_{pv}+I_sR_S)}{(N_SAKT)}} - 1] \tag{2.6}$$

The typical I-V output characteristics of P-V cell is represented by following equations [7]:

Module photo-current (I_{ph}):

$$I_{ph} = \frac{[I_{scr} + K_i(T - 298)]G}{1000} \tag{2.7}$$

Module reverse saturation current (I_{rs}):

$$I_{rs} = \frac{I_{scr}}{e^{(qV_{oc}/N_sKAT)} - 1} \tag{2.8}$$

Module saturation current (I_o):

$$I_o = I_{rs}\left[\frac{T}{T_r}\right]^3 e^{\frac{qE_{go}}{BK(\frac{1}{T_r} - \frac{1}{T})}} \tag{2.9}$$

The current output of PV-module (I_{pv}):

$$I_s = I_{ph} - I_o[e^{\frac{q(V_{pv}+I_sR_S)}{(N_SAKT)}} - 1] \tag{2.10}$$

2.2.3 Improved single Diode Model (I_mSDM):

The improved Single Diode Model is based on the idealized Ideal Single Diode Model. However, in order to cope up with the mathematical complexity it is modeled with an entirely different set of mathematical equations. The computation of these equations avoids the use of a non-linear solver [9]. In the Improved Single Diode Model the effects of R_s and R_{sh} are neglected for mathematical simplicity. The equation (2.1) reduces to:

$$I_{pv} = I_{ph} - I_o\left[e^{\left(\frac{qV_{pv}}{N_sKTA}\right)} - 1\right] \tag{2.11}$$

This model basically contains three unknown parameters namely I_{ph}, I_o and A.

We know that

$$V_{oc}(G,T)-V_{oc}(G,T_0)=-|\beta|\Delta T \tag{2.12}$$

Where $V_{oc}(G,T)$ represents the open circuit voltage at T and $V_{oc}(G,T_0)$ represents the open circuit voltage at the reference temperature.

The open circuit voltage formula is derived by substituting I=0 in (2.11)

$$V_{oc}=\frac{N_s KTA}{q}\ln\left(\frac{I_{ph}}{I_o}+1\right) \tag{2.13}$$

Substituting for $V_{oc}(G,T)$ and $V_{oc}(G,T_0)$ in eq (13) we get

$$\frac{N_s KTA}{q}\left[T\ln\left(\frac{G(I_{sc}+K_i\Delta T)}{I_o}+1\right)-T_0\ln\left(\frac{GI_{sc}}{I_{rs}}+1\right)\right]=-|\beta|\Delta T \tag{2.14}$$

Rearranging the above equation we get

$$I_o=\frac{e^{\frac{|\beta|\Delta Tq}{N_s KTA}}\left(G(I_{sc}+K_i\Delta T)\right)}{\left(GI_{sc}/I_{rs}+1\right)^{\frac{T_0}{T}}-e^{\frac{|\beta|\Delta Tq}{N_s KTA}}} \tag{2.15}$$

Here we have I_{rs}which can be found by

$$I_{rs}=\frac{I_{sc}}{\left(e^{\frac{qV_{oc}}{N_s KAT_0}}-1\right)} \tag{2.16}$$

Furthermore, the equation for the MPP under STC can be expressed as

$$I_m=I_{sc}-I_{rs}\left(e^{\frac{qV_m}{N_s KAT_0}}-1\right) \tag{2.17}$$

Now the unknown parameter A can be derived by substituting (2.16) into (2.17)

$$\frac{I_m}{I_{sc}}=e^{\frac{qV_m}{N_s KAT_0}}-\left(\frac{I_{sc}-I_m}{I_{sc}}\right)e^{\frac{qV_{oc}}{N_s KAT_0}} \tag{2.18}$$

Thus we can find the unknowns A and I_{sc}

Now I_{ph} is determined by the equation

$$I_{ph} = G\left(I_{sc} + K_i \Delta T\right) \tag{2.19}$$

where G the incident irradiance (kW/m2) , $I_{sc}$is the short circuit current at STC (in A), ΔT is the temperature difference between the module temperature and the STC temperature, and K_i is the current temperature coefficient.

Finding the value of the unknowns and replacing in (2.11) we get the exact modelling of the improved single diode model.

2.2.4 Single Diode Model with R_s and R_{sh} (SDM)

From the Fig.2.3, we include the effect of both R_s and R_{sh}. The equation can be written basically through three points as specified on the data sheet namely the short circuit point, the maximum power point and the open circuit point.

$$I_{sc} = I_{ph} - I_{rs}\left[e^{\left(\frac{qI_{sc}R_sN_s}{N_sKTA}\right)} - 1\right] - \left(\frac{I_{sc}R_s}{R_{sh}}\right) \tag{2.20}$$

$$I_{mpp} = I_{ph} - I_o\left[e^{\left(\frac{q\left(V_{mpp}+I_{mpp}R_sN_s\right)}{N_sKTA}\right)} - 1\right] - \left(\frac{\left(V_{mpp}+I_{mpp}R_sN_s\right)}{N_sR_{sh}}\right) \tag{2.21}$$

$$I_{oc} = I_{ph} - I_o\left[e^{\left(\frac{qV_{oc}}{N_sKTA}\right)} - 1\right] - \left(\frac{V_{oc}}{N_sR_{sh}}\right) \tag{2.22}$$

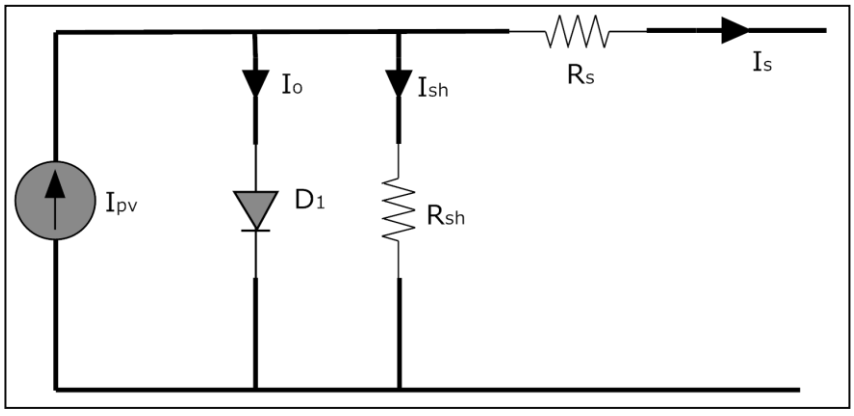

Fig.2.3. PV cell modeled as single diode circuit including R_s and R_{sh}

Another equation can also be derived using the fact that, at the MPP, the slope of the P-V curve is zero.

$$\frac{dP}{dV} = 0 \text{ at MPP} \tag{2.23}$$

So far there are four equations available, but there are five parameters to find, therefore a fifth equation has to be found. For this purpose can be used the derivative of the current with the voltage at short-circuit conditions, which is mainly determined by the shunt resistance R_{sh}.

$$\frac{dI}{dV} = \frac{-1}{R_{sh}} \text{ at } I=I_{sc} \tag{2.24}$$

From the expression of the current at short-circuit and open circuit conditions, the photo-generated current I_{ph} and the saturation current I_o can be expressed:

$$I_{ph} = I_o\left[e^{\left(\frac{qV_{oc}}{N_sKTA}\right)} - 1\right] - \left(\frac{V_{oc}}{N_sR_{sh}}\right) \tag{2.25}$$

From eq.(2.25) and (2.20) we get

$$I_{sc} = I_o\left[e^{\left(\frac{qV_{oc}}{N_sKTA}\right)} - e^{\left(\frac{qI_{sc}R_sN_s}{N_sKTA}\right)}\right] - \left(\frac{V_{oc} - I_{sc}R_s}{N_sR_{sh}}\right) \tag{2.26}$$

The second term in the parenthesis from the above equation is neglected as it is very less compared to the first term.

$$I_{sc} = I_o e^{\left(\frac{qV_{oc}}{N_sKTA}\right)} - \left(\frac{V_{oc} - I_{sc}R_s}{N_sR_{sh}}\right) \tag{2.27}$$

Solving for the saturation current we get

$$I_o = I_{sc} - \left(\frac{V_{oc} - I_{sc}R_s}{R_{sh}}\right)e^{\left(\frac{-qV_{oc}}{N_sKTA}\right)} \tag{2.28}$$

Combining equation (2.25) (2.28) and (2.21) we get

$$I_{mpp} = I_{sc} - \frac{V_{mpp} + I_{mpp}R_s - I_{sc}R_s}{R_{sh}} - \left(I_{sc} - \frac{V_{oc} - I_{sc}R_s}{R_{sh}}\right)e^{\frac{q\left(V_{mpp}+I_{mpp}R_s-V_{oc}\right)}{N_sKAT}} \tag{2.29}$$

Now we apply the maximum power point (MPP);

$$\frac{dP}{dV} = I + \frac{dI}{dV}V \tag{2.30}$$

In order to obtain the derivative of the power at MPP, the derivative of Eq. (2.29) with voltage should be found. However, since (2.29) is a transcendental equation, and it is expressed in the form

$$I = f(I,V) \tag{2.31}$$

Differentiating we get

$$dI = dI\frac{\partial f(I,V)}{\partial I} + dV\frac{\partial f(I,V)}{\partial V} \tag{2.32}$$

$$\frac{dI}{dV} = \frac{\frac{\partial}{\partial V}f(I,V)}{1-\frac{\partial}{\partial I}f(I,V)} \tag{2.33}$$

From (2.33) and (2.30)

$$\frac{dP}{dV} = I_{mpp} + \frac{V_{mpp}\frac{\partial}{\partial V}f(I,V)}{1-\frac{\partial}{\partial I}f(I,V)} \tag{2.34}$$

From the above equations

$$\frac{dP}{dV}|_{I=\mathrm{Im}\,pp} = I_{mpp} + V_{mpp}\frac{-\frac{(I_{sc}R_{sh}-V_{oc}+I_{sc}R_s)e^{\frac{Vmpp+\mathrm{Im}\,ppRs-V_{oc}}{NsV_t}}}{N_sV_tR_{sh}} - \frac{1}{R_{sh}}}{1+\frac{(I_{sc}R_{sh}-V_{oc}+I_{sc}R_s)e^{\frac{V_{mpp}+I_{mpp}R_s-V}{NsV_t}}}{N_sV_tR_{sh}} + \frac{R_s}{R_{sh}}} \tag{2.35}$$

These equations lead to the equation:

$$\frac{-1}{R_{sh}}|_{I=Isc} = \frac{-\frac{(I_{sc}R_{sh}-V_{oc}+I_{sc}R_s)e^{\frac{IscRs-V_{oc}}{NsV_t}}}{nsV_tR_{sh}} - \frac{1}{R_{sh}}}{1+\frac{(I_{sc}R_{sh}-V_{oc}+I_{sc}R_s)e^{\frac{I_{sc}R_s-V}{NsV_t}}}{nsV_tR_{sh}} + \frac{R_s}{R_{sh}}} \tag{2.36}$$

Now we can determine all the three unknown parameters, the R_s, A, and R_{sh} using the equations. As these equations do not allow separating the unknowns, they are solved using numerical methods.

2.2.5 Two Diode Model

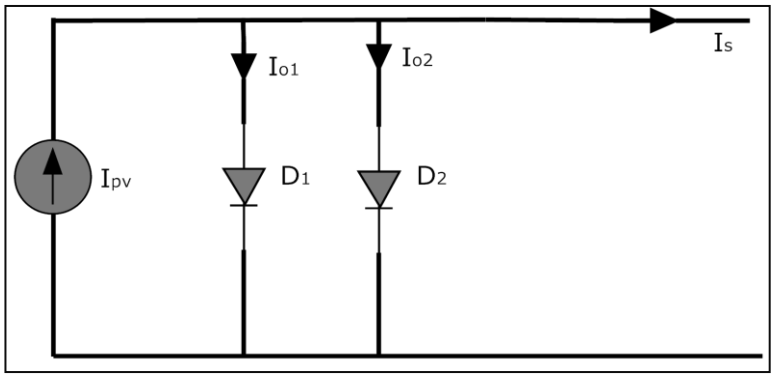

Fig.2.4. PV cell modelled as two diode circuit

For Two Diode Model, we considered two diodes as shown in the Fig.2.4 which consists of two parallel diodes instead of a single diode as before. It led to increase in accuracy of the model with greater resemblance to experimental data. This model is known to have better accuracy at low irradiance level which allows for a more accurate prediction of PV system performance [12]. To reduce computational time, the input parameters are reduced. Here R_s and R_{sh} are excluded for simplicity.

The output current of the cell may be described as

$$I_{pv} = I_{ph} - I_{d1} - I_{d2} \tag{2.37}$$

where I_{d1} is the current through diode d_1 and is given by

$$I_{d1} = I_{01}\left[e^{\frac{V_{pv}}{A_1 V_{T1}}} - 1 \right] \tag{2.38}$$

And I_{d2} is the current through diode d_2 which is given by

$$I_{d2} = I_{02}\left[e^{\frac{V_{pv}}{A_2 V_{T2}}} - 1 \right] \tag{2.39}$$

Where I_{o1} is the reverse saturation current of diode 1 and $I_{02}$is the reverse saturation currents of diode 2, $V_{T1}$and $V_{T2}$are the thermal voltages of diode 1 and diode 2 respectively. A_1 and A_2represent the diode ideality factors. It requires the computation of five parameters, namely I_{PV}, I_{o1}, I_{02}, a_1 and a_2. To simplify, several researchers assumed a_1=1 & a_2=2.

2.2.6 Improved Simplified Single Diode Model

The I-V characteristics of the PV device depend on its internal characteristics (R_S, R_P) and on the external influences such as irradiation level and temperature. The model has four parameters (I_{PH}, I_S, A, R_S). As the parallel resistance is high, for simplicity, I_{SC} is assumed to be equal to I_{PV}.

Generally, the I-V characteristics for a PV module composed of series connected cells based on single exponential model is expressed as

$$I_S = I_{PV} - I_o\left[\exp(q(V_{PV} + I_S R_S)/AKTN_S) - 1\right] \tag{2.40}$$

The light-generated current of the PV cell depends linearly on the solar irradiation and is affected by the change in surrounding temperature.

The module photocurrent is given by:

$$I_{PV} = (I_{SC} + K_I \Delta T)G \tag{2.41}$$

The nominal saturation current at standard temperature and irradiation is given by:

$$I_{RS} = \frac{I_{SC}}{\exp(V_{OC,N}/AKN_S T_0) - 1} \tag{2.42}$$

The PV model proposed in [8] is improved by replacing the conventional approach of obtaining the saturation current by the equation:

$$I_O = \frac{I_{SC} + K_I \Delta T}{\exp((V_{OC,N} + K_V \Delta T)/AKN_s T) - 1} \tag{2.43}$$

This modification aims to match the open-circuit voltages of the model with the experimental data for a wide variation in temperature. The inclusion of current and voltage coefficient K_I and K_V in (2.42) gives (2.43). The above equation gives a new approach of dependency of I_o in temperature such that, the temperature is a linear variation of the open-circuit voltage (V_{OC}).

Under Standard Temperature Conditions (STC), at MPP point (I_{MPP},V_{MPP}) equation (2.40) is given by:

$$I_{MPP} = I_{SC} - I_{RS}[\exp(q(V_{MPP} + I_{MPP}R_S)/AKT_oN_s) - 1] \quad (2.44)$$

The third parameter "*A*" is derived by substituting (2.42) in (2.44) and solving

$$\frac{I_M}{I_{SC}} = \exp(q(V_M + I_M R_S)/AKN_S T_o) - (\frac{I_{SC} - I_M}{I_{SC}})\exp(qV_{OC}/AKN_S T_o) \quad (2.45)$$

The series resistance R_S which represents the resistance inside each cell in the connection between cells, gives a more accurate shape between the maximum power point and the open-circuit voltage.

The fourth unknown parameter is given by:

$$R_S = -\frac{dV}{dI_{V_{OC}}} - \frac{1}{X_V} \quad (2.46)$$

$$X_V = I_{RS}(q/AKT_o)\exp(qV_{OC}/AKT_o) \quad (2.47)$$

$$\frac{dV}{dI_{V_{OC}}} = 1.15/N_s/2 \quad (2.48)$$

Solving (2.45) and (2.46) we can obtain the value of the unknown parameters. The inclusion of unknown parameter results in closer resemblance of the simulated model to the practical PV array, thus improving the output characteristic curve and minimizing the error at the remarkable points of the curve.

2.3 SIMULATION RESULTS

2.3.1 Analysis of P-V_{pv} and I_{pv}-V_{pv} Curves

Fig. 2.5 and Fig.2.6 depict the typical P-V and I-V characteristics of various PV models at a particular temperature and irradiation. From this, following interpretations are made. The output curve for *an ideal single diode model* doesn't guarantee accurate shape between the maximum power point and the open-circuit voltage because of the exclusion of R_s and also because of the exclusion of R_{sh}. Hence the graphs deviates completely from the experimental results obtained. For the *single diode model with R_s only*, the model is improved. The graph obtained coincides with the experimental result at I_{sc} and V_{oc} but the MPP deviates greatly for the one obtained from experimental result. It even exhibits serious deficiencies when subjected to temperature variations. For the *single diode model considering both R_s and R_{sh}*,

the model is significantly improved and is almost approximated to the actual PV panel but, this approach demands significant computing effort and its accuracy deteriorates at low irradiance, especially in the vicinity of V_{oc} . For the *two diode model***,** the graph deviates from the experimental result near the vicinity of I_{sc} but the graph has MPP near to the experimental MPP and the graph between the MPP and V_{oc} is near to the experimental result. However, for the *improved single diode model***,** the simulation result coincides closely with the experimental result and exactly at MPP. It takes advantage of the simplicity of ideal models and enhances the accuracy by deriving a mathematical representation, capable of extracting accurate estimates of the model parameters, directly related to manufacturer datasheets.

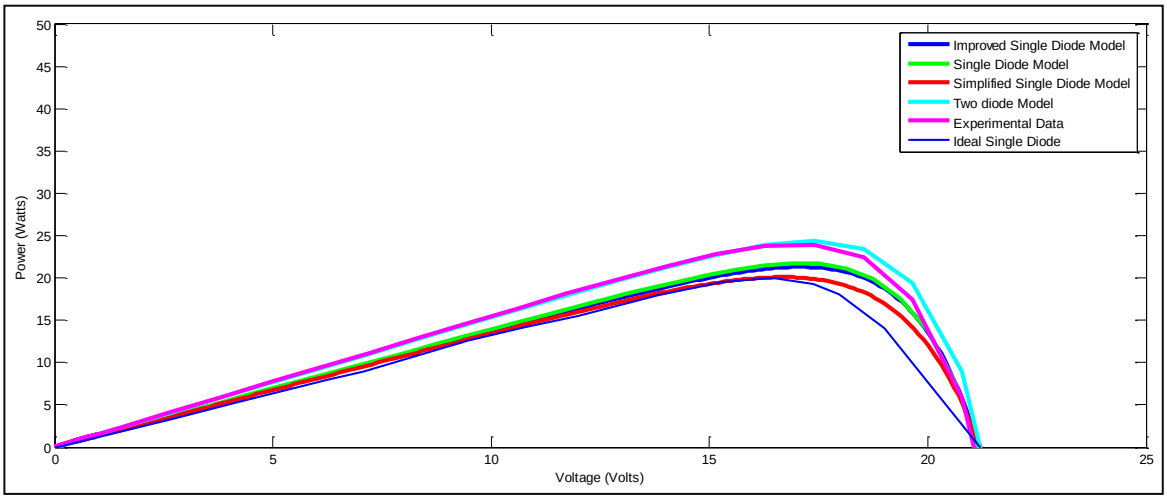

Fig.2.5. Typical P-V_{pv} output characteristics for different PV equivalent circuits at a particular irradiation and temperature

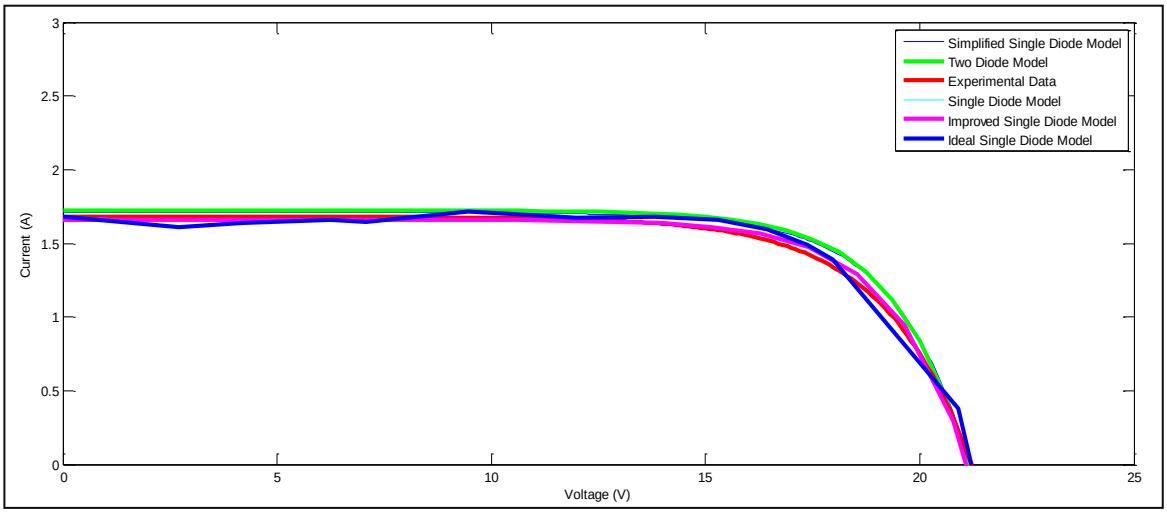

Fig.2.6. Typical I_{pv}-V_{pv} output characteristics for different PV equivalent models at a particular temperature and irradiation

2.3.2 Analysis of the RMSD values

Table-2.1 gives the Root Mean Square Deviation (RMSD) comparison between the various PV models and thus the result clearly shows the order of preference of the model in order to get the approximate graph coinciding closely to the experimental datasheet values at MPP, V_{oc}, I_{sc}..However, the most accurate model is obtained by using the two diode model including R_s and R_{sh}. But because of the tremendous increase in the computation complexity involving seven parameters, its not used for study. Table-2.2 illustrates the point at which MPP is obtained.

TABLE-2.1 RMSD values for different PV equivalent circuits

Equivalent Circuit	*RMSD*
Ideal single diode	0.089(A)
With R_s (SSDM)	0.068(A)
With R_s and R_{sh} (SDM)	0.056(A)
With two-diode	0.0547(A)
With improved single diode	0.053(A)

TABLE-2.2 MPP values for different PV equivalent circuits

Equivalent Circuit	*MPP*
Ideal single diode	16.1(V), 1.42(A)
With R_s(SSDM)	16.68(V), 1.51(A)
With R_s and R_{sh}(SDM)	16.29(V), 1.46(A)
With two-diode	16.31(V), 1.47(A)
With improved single diode	16.30(V), 1.47(A)

CHAPTER 3

Soft Switching DC-DC Boost Converter for PV Applications

3.1 INTRODUCTION

Hard Switching converters comprise of those converters which obeys the conventional switching phenomenon. While the switch is turned ON, the voltage across the switch tends to decrease and the current across the switch tends to increase. This results in some switching losses.

Switching losses and EMI can be reduced by using soft switching techniques at the expense of stress on the device. If the semiconductor device is made to turn off or turn on when current or voltage is zero, then the product of voltage and current during transition is zero which leads to zero power loss.

3.2 MATHEMATICAL ANALYSIS OF SOFT SWITCHING BOOST CONVERTER

The following assumptions are made for the operation and the analysis of the converter: (a) Output capacitance is large enough to obtain constant output voltage (b) Main inductor is large enough to have input current constant.

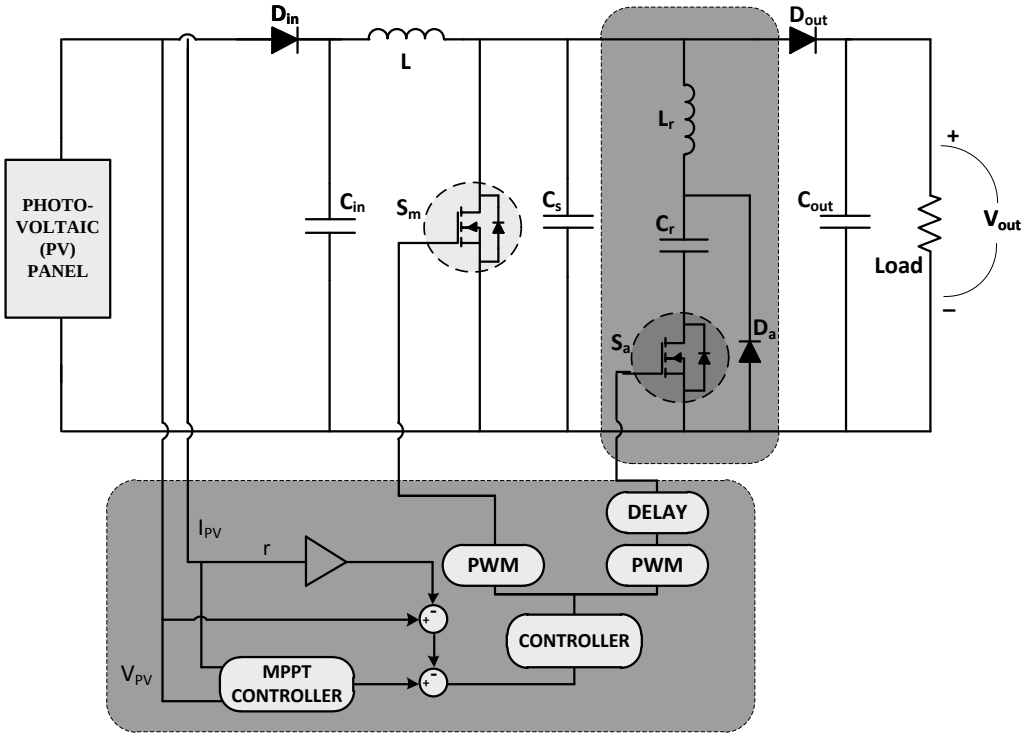

Fig. 3.1. The Soft Switching Boost Converter Topology

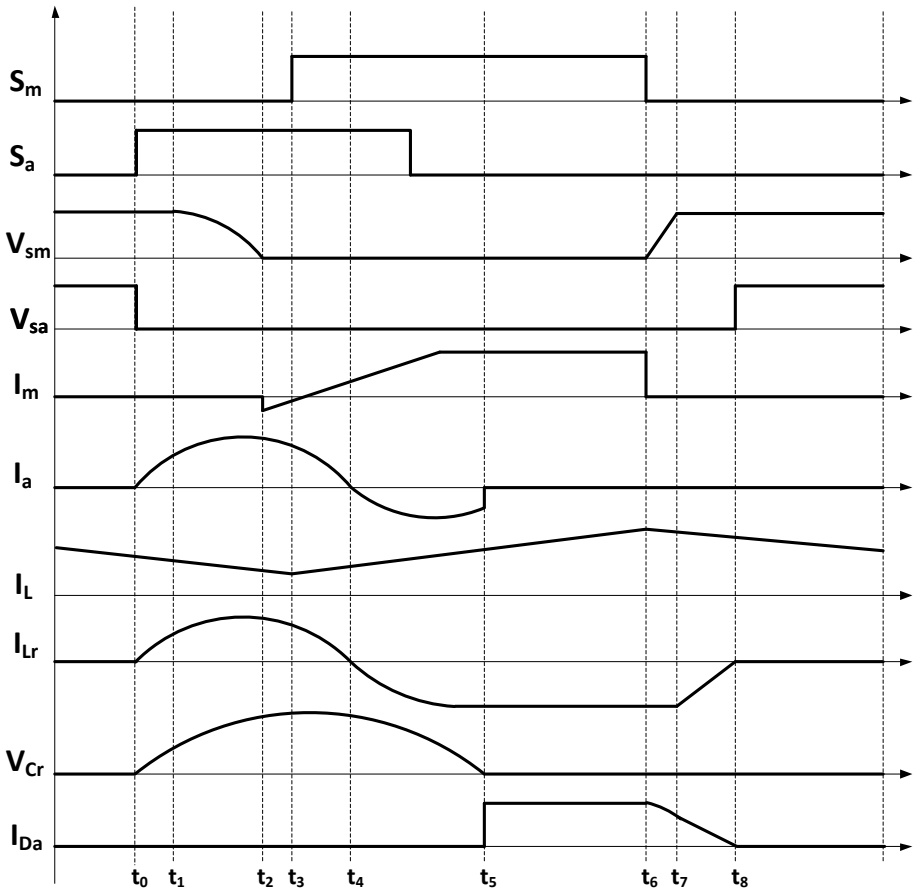

Fig. 3.2 Theoretical Waveforms of the Soft Switching Converter

3.2.1 Analysis of various modes of operations

A. Mode 1(t_0-t_1):

At the beginning of this stage, the auxiliary switch S_a is turned on with ZCS while the main switch is off. A resonant loop consisting of L_m-L_r-C_r-S_a-V_{in} is formed because of the resonance between L_r and C_r. The current in D_a reaches zero (soft turn-off) at the end of the interval. Now, when the current through L_m equals to the current through L_r, mode 1 ends. The voltages and currents are derived using KVL and KCL.

The power loss in this interval is due to the conduction loss due to the switch S_a(P_{Sa}) and the main diode D_{out} (P_{Dout}) and they are given by:

$$P_{s_a} = (i_{s_a}\,|_{t_1})^2 * R_{m_{2on}} * \left(\frac{t_1 - t_0}{3T}\right) \tag{3.1}$$

$$P_{D_{out}} = \frac{0.7 * i_o * (t_1 - t_0)}{2T} \tag{3.2}$$

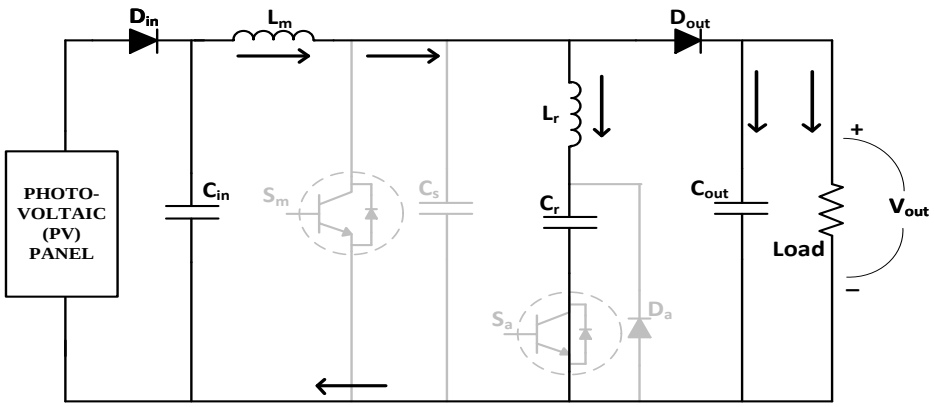

B. Mode 2(t_1-t_2):

In this interval, switch S_a remains on and the current through L_r increases due to the resonance between L_r and C_r. The drain voltage of main switch S_m starts to drop as the snubber capacitor discharges. This mode ends when the voltage of C_s drops to zero.

The power loss in this mode is mainly due to the conduction loss in the switch S_a(P_{Sa}):

$$P_{s_a} = (i_{s_a}|_{t_2})^2 * R_{m_{2on}} * \left(\frac{t_2 - t_1}{3T}\right) \tag{3.3}$$

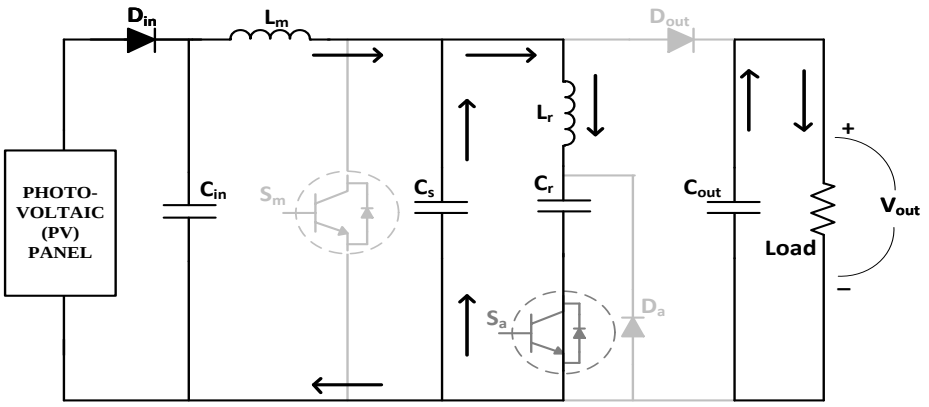

C. Mode 3(t_2-t_3):

At the beginning of this interval, the anti-parallel diode of the main switch S_m is turned on, which makes the voltage across main switch zero by ZVS turn-on. This mode ends when the current through main inductor equals that of the resonant inductor current.

The power loss in this mode is due to the conduction loss of both switch S_a(P_{Sa}) and the anti-parallel diode of switch S_m(P_{Sm}) and they are given by:

$$P_{s_a} = (i_{s_a}|_{t_3})^2 * R_{m_{2on}} * \left(\frac{t_3 - t_2}{3T}\right) \tag{3.4}$$

$$P_{D_{s_m}} = \frac{0.7 * i_{s_m} * (t_3 - t_2)}{2T} \tag{3.5}$$

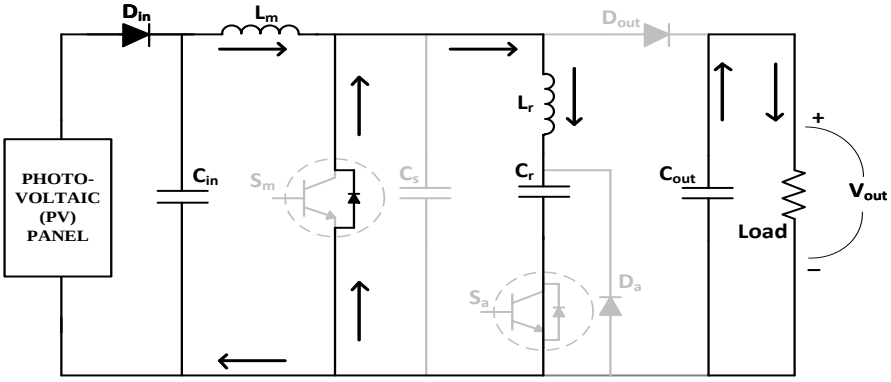

D. Mode 4(t_3-t_4):

Here, in this mode, the main switch S_m is turned on at zero voltage condition and hence, there is no switching loss across it. The resonant capacitor is charged continuously in this mode. The load current is provided by the output capacitor.

The power losses in this interval include conduction loss in main switch S_m (P_{Sm}) as well as auxiliary switch S_a(P_{Sa}):

$$P_{s_m} = (i_{L_m}|_{t_4})^2 * R_{m_{on}} * \left(\frac{t_4 - t_3}{3T}\right) \tag{3.6}$$

$$P_{s_a} = (i_{s_a}|_{t_4})^2 * R_{m_{2on}} * \left(\frac{t_4 - t_3}{3T}\right) \tag{3.7}$$

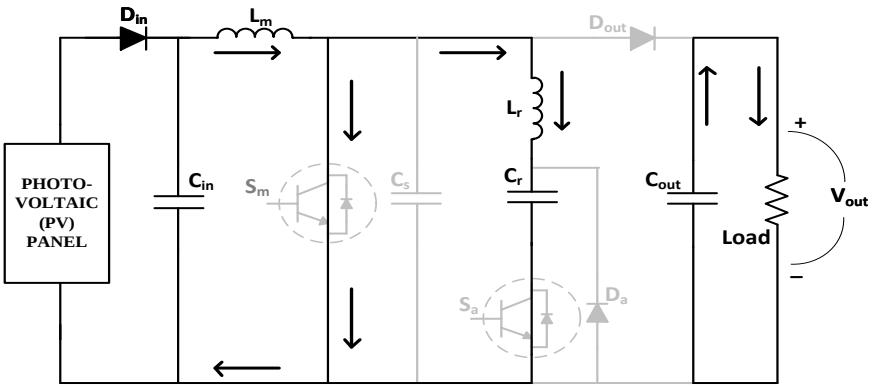

E. Mode 5(t_4-t_5):

In this mode, the current flows through the anti-parallel diode of S_a. Hence, the switch S_a is turned off under ZVS. Thus, there is no switching loss in S_a during turn-off. This mode ends when resonant capacitor C_r is fully charged.

The power loss in this interval is due to the conduction loss across switch S_m(P_{Sm})and the anti-parallel diode of switch S_a(P_{Dsa}).

$$P_{s_m} = (i_{s_m}|_{t_5})^2 * R_{m_{on}} * \left(\frac{t_5 - t_4}{3T}\right) \tag{3.8}$$

$$P_{D_{s_a}} = \frac{0.7 * i_{s_a} * (t_5 - t_4)}{2T} \tag{3.9}$$

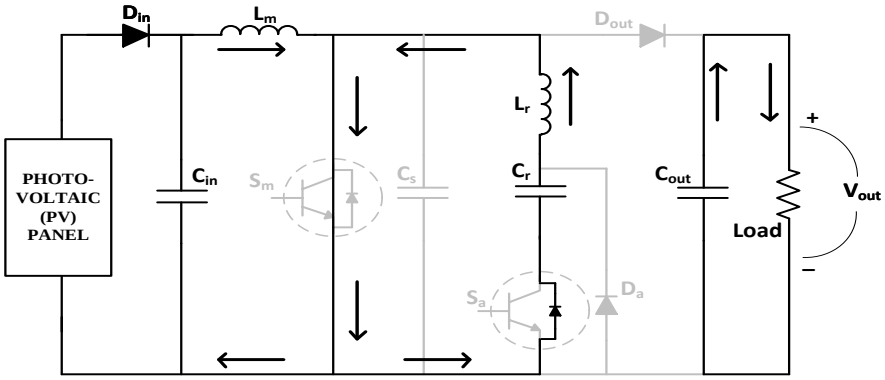

F. Mode 6(t_5-t_6):

In this interval, the current flows through the auxiliary diode D_a instead of the anti-parallel diode of switch S_a. This mode ends when the main switch S_m is turned off.

Here, the power loss is influenced by the switching loss of the auxiliary diode D_a($P_{Da\text{-}sw}$) and the conduction loss across switch S_m(P_{Sm}) and D_a(P_{Da}).

$$P_{s_m} = (i_{s_m}|_{t_6})^2 * R_{m_{on}} * \left(\frac{t_6 - t_5}{3T}\right) \tag{3.10}$$

$$P_{D_a} = \frac{0.7 * i_{L_r}|_{t_6} * (t_6 - t_5)}{2T} \tag{3.11}$$

$$P_{D_a - sw} = \frac{0.7 * i_{L_r}|_{t_6} * (t_6 - t_5)}{2T} \tag{3.12}$$

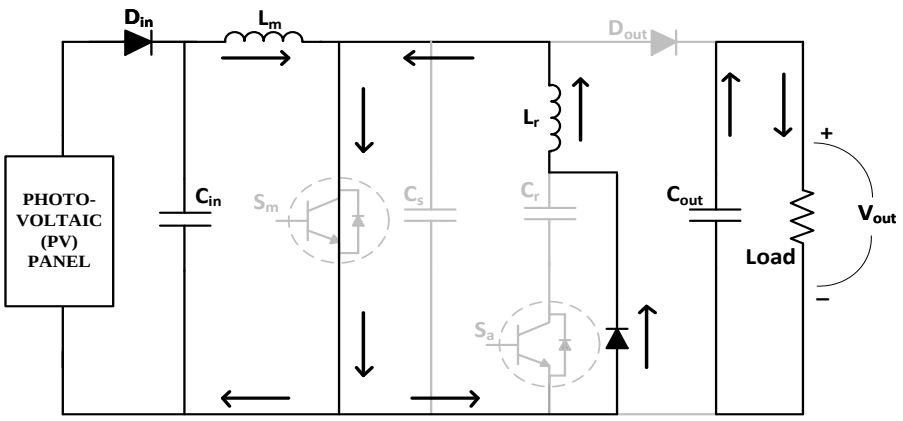

G. Mode 7(t_6-t_7):

In this mode, the main switch S_m is turned off under ZVS condition by the help of the snubber capacitor C_s. The energy is stored in the capacitor C_s. This mode ends when C_s is fully charged.

Since, the main switch is turned off under ZVS, the switching loss across S_m is zero and the entire loss is contributed by the conduction loss of D_a(P_{Da})

$$P_{D_a} = \frac{0.7 * i_{L_r} \mid t_7 * (t_7 - t_6)}{2T} \tag{3.13}$$

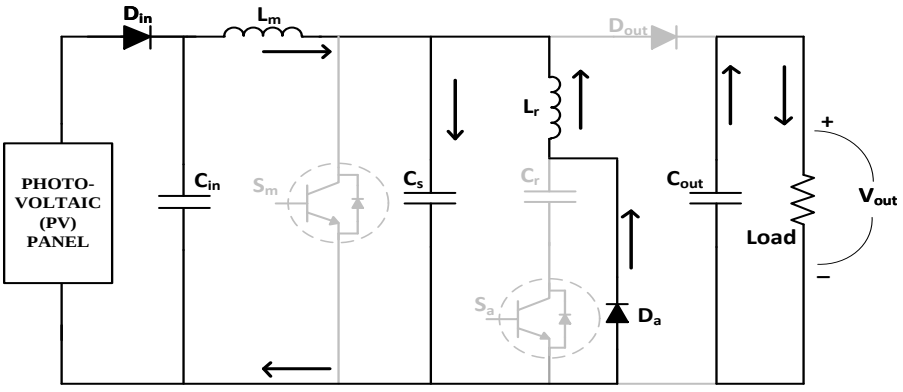

H. Mode 8(t_7-t_8):

Here, in this mode, the resonant inductor L_r starts discharging and the energy is transferred to the load through the output diode (D_{out}). This mode comes to an end when L_r is discharged completely. Because of the ZVS condition, D_{out} doesn't experience any switching loss and the power loss is due to the conduction loss across D_a and D_{out}.

$$P_{D_{out}} = \frac{0.7 * i_o \mid_{t_8} (t_8 - t_7)}{2T} \tag{3.14}$$

$$P_{D_a} = \frac{0.7 * i_{L_r} \mid_{t_8} * (t_8 - t_7)}{2T} \tag{3.15}$$

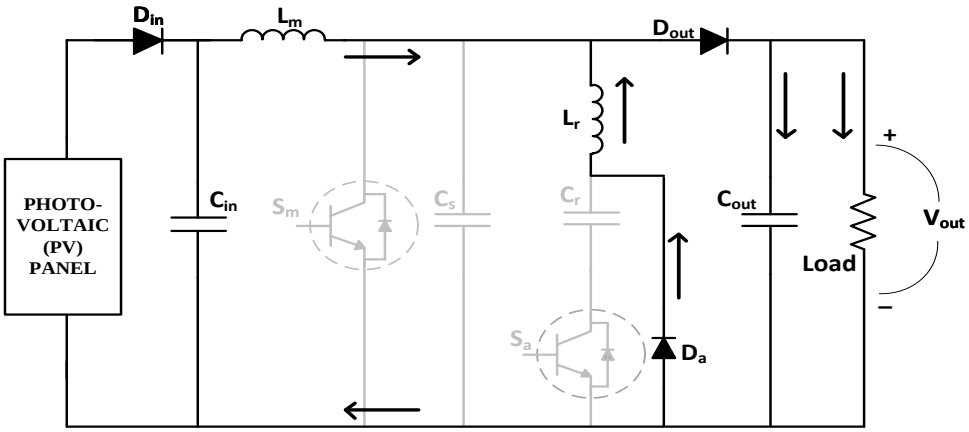

I. Mode 9 (t_8-t_9):

In this interval, all the switches are turned off and the entire current flows through the D_{out} to the load. Hence this mode ends when S_a is turned on.

The power loss is contributed by the switching loss of D_a($P_{Da\text{-}sw}$) and the conduction loss of D_{out} (P_{Dout}).

$$P_{D_{OUT}} = \frac{0.7 * i_o \mid_{t_9} (t_9 - t_8)}{2T} \tag{3.16}$$

$$P_{D-off} = \frac{V_o * i_{Arr} * t_{Arr}}{4T} \tag{3.17}$$

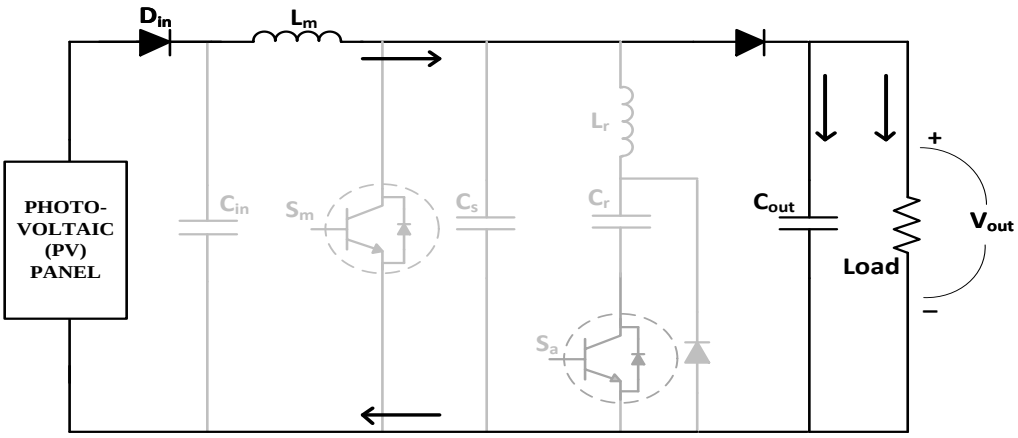

3.3 THEORY OF MAIN SWITCH AND AUXILIARY SWITCH

The auxiliary switch operates with such a duty ratio that enables the main switch to operate with soft switching. If the auxiliary switch is turned on, the resonant loop of the resonant inductor (L_r) and resonant capacitor (C_r) is made. ZVS area is guaranteed by turning on the auxiliary switch. The PWM pulses have to be made with a delay between the main switch and the auxiliary switch. A phase-difference can be obtained by delaying the carrier waveform. Points at which the switches turn on have to be fixed in order to realize soft-switching with resonance. The minimum delay time must satisfy the equation.

$$T_{Delay} \geq \frac{I_{in} L_r}{V_o} + \frac{\pi}{2}\sqrt{L_r C_r} \tag{3.18}$$

During the delay time, the auxiliary switch is turned ON. From the volt-second balance for the main inductor, the voltage-conversion ratio is defined by:

$$\frac{V_o}{V_{in}} \approx \frac{1}{1-(D_{aux}+D_{main})} \tag{3.19}$$

where, D_{aux} is the auxiliary switch duty ratio and D_{main} is the main switch duty ratio.

3.4 INDUCTOR DESIGN FOR PRACTICAL IMPLEMENTATION

The initiation of the design procedure starts with the determination of the input parameters for the design. Various parameters involved are the selection of topology, output power, switching frequency, DC output voltage, minimum input voltage, maximum input voltage, maximum temperature, efficiency of the inductor and efficiency of the pre-regulator [1]. We know,

$$P_{tot} = (1-\eta_L)(P_{out}/\eta_{preg}) \tag{3.20}$$

$$P_{core} = P_{tot}/2 = P_{Cu} \tag{3.21}$$

Loss per core weight and core loss are given by

$$P_I = P_{tot}/weight \tag{3.22}$$

$$P_{coreloss} = 6.5 f_{sw}^{1.51}.B_{ac}^{1.74} \tag{3.23}$$

The calculation of the critical value of inductor hasn't been mentioned in details for brevity. However, we know the value of the input current. The energy storage requirement of the inductor is now calculated using the formulae

$$E = 0.5 L_{critical} I^2_{peakinput} \tag{3.24}$$

The number of turns required is given by the following expressions.

$$N = \frac{L_{critical}.I_{inputcritical} * 10^4}{B_{\max} A_c} cm^2 \tag{3.25}$$

In the laboratory, the inductor was made by taking a core TDK 5523 PC40Z with 43 turns.

CHAPTER 4

Results and Discussions

The designed boost converter along with the PV panel and a control tracker for MPPT algorithm is simulated using PSIM 64 bit version 9.0. Table 4.1 shows the values of all the parameters used in the simulation and design of the converter. The simulation is performed under a 30 kHz switching frequency and a rated power of 36 W.

TABLE 4.1 : PARAMETERS USED IN SIMULATION

Parameter	*Label*	*Value*
Output Voltage	V_{out}	45 V
Rated Power	P_{rated}	36 W
Main inductor	L	5.6 mH
Resonant Inductor	L_r	10 uH
Resonant Capacitor	C_r	100 nF
Snubber Capacitor	C_s	20 nF
Switching Frequency	f_{sw}	30 kHz
Input Capacitor	C_{in}	4.9 nF
Ripple Factor	*R.F.*	25 %

The PV array has an operating voltage of 18 V. The inclusion of series resistance and ideality factor as unknown parameters for PV modeling aided in the smoothness of the output characteristics between MPP and open-circuit voltage and thus, coincides closely with the experimental data obtained. The experiment is performed at 540 W/m^2 and at 37^{o}C. Table4.2 shows the components used in the experimental set up of the converter.

TABLE 4.2 : COMPONENTS USED IN THE PROTOTYPE

Components	*Devices*
Main Switch	IRF54CN
Auxiliary Switch	IRF54CN
Main Inductor	Wound-type
Resonant Inductor	Wound-type
Output Diode	1N4007S
Auxiliary Diode	1N4007S

4.1 SIMULATION RESULTS

Simulation results of the main switch voltage and current waveforms shown in Fig. 4.1(b) depicts the ZVS turn on and turn off. The turning on of the anti-parallel diode of the main switch and the slope of the voltage provided by the snubber capacitor are responsible for the same.

The auxiliary switch voltage and current waveforms have been shown in Fig.4.1(c). The resonance between the inductor and the capacitor and the reversing of the inductor current leads to the turn on of the switch by ZCS. The anti-parallel diode present is responsible for the ZVS turn off of the auxiliary capacitor. Perturb and Observe (P&O) Method has been applied to extract the MPP and the duty ratio is fed to the main and auxiliary switch of the boost converter. The current through the input inductor which was assumed to be constant, has a small amount of ripple present which has been accounted for.

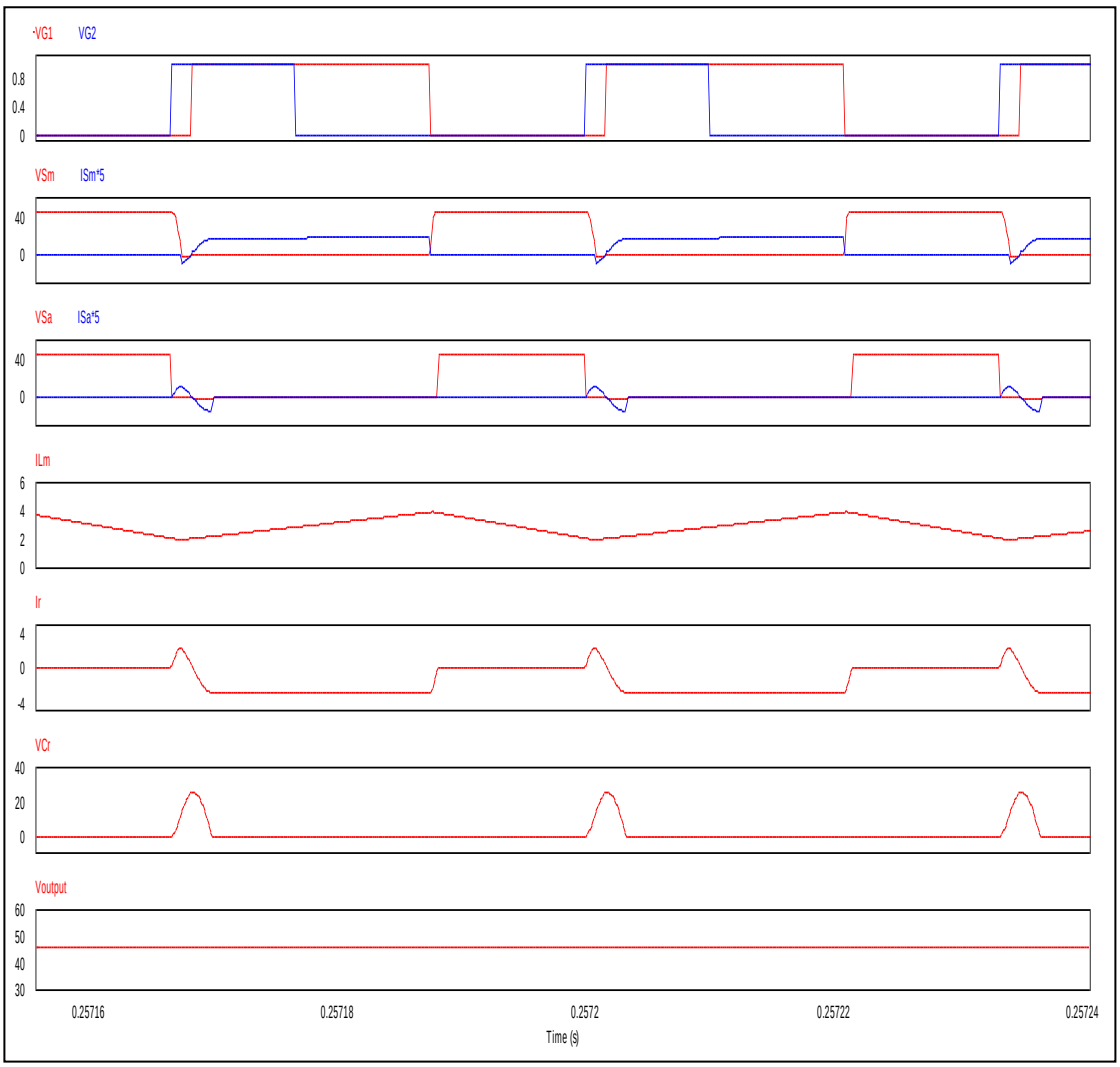

Fig. 4.1. Simulation waveforms : Gating Signals ,Voltage and Current across main switch ,Voltage and Current across auxiliary switch, Current through input inductor L ,Current through resonant inductor L_r, Voltage across resonant Capacitor and Output Voltage

4.2 EXPERIMENTAL VALIDATION

The experimental setup for the soft-switching Boost Converter along with the PV panel and load and FPGA Kit for pulse generation is shown in Fig. 4.2. The experimental results of the converter design have been shown in Fig.4.3. The input and output voltages are shown in the Fig. 4.3(a) and 4.3(b) which shows a considerable boost to around 45 V at the output with an input of 18 V to it. The turning on of the main switch leads to the storage of energy in the main inductor L_m, which is transferred to the output when the switch is turned off.

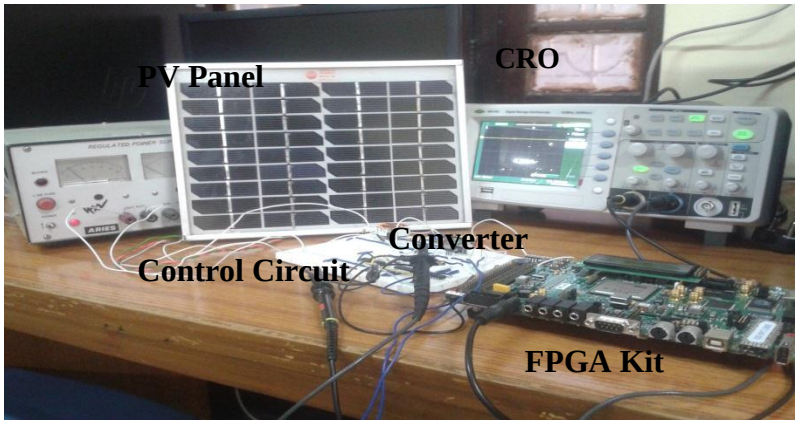

Fig. 4.2. Prototype of the soft switching boost converter

The main switch ZVS Turn-On has been shown in the Fig. 4.3(c). The current becomes negative on account of its flow through the antiparallel diode during the turning on condition. This leads to a zero voltage across the switch and thus making ZVS possible across the main switch. It is seen that there is a reduction in the overlap between the current and the voltage waveforms thus leading to reduced switching losses. The switching loss is adjustable by adjusting the value of the snubber capacitor and it is so chosen so as to minimize the losses. The auxiliary switch ZCS Turn-On and ZVS Turn-Off has been shown in Fig. 4.3(d). The current has a nearly sinusoidal nature at the switching instant.

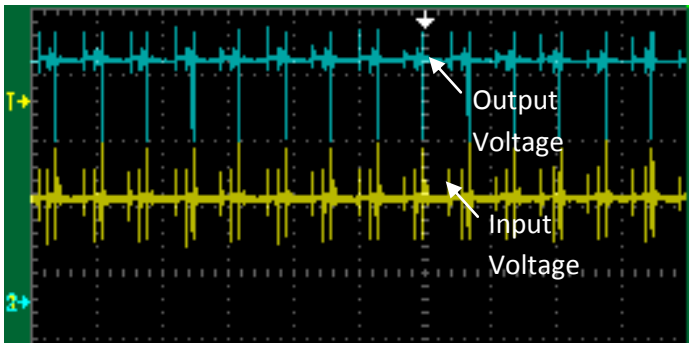

(a)

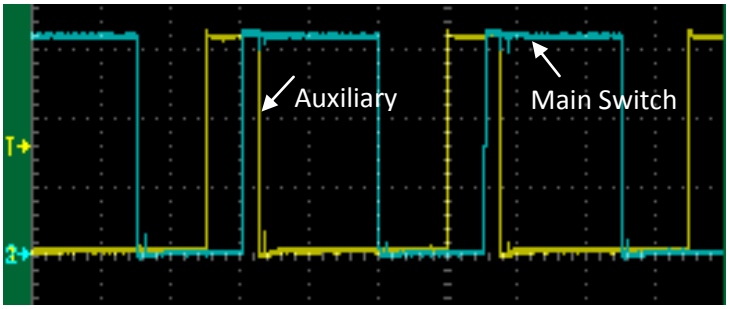

(b)

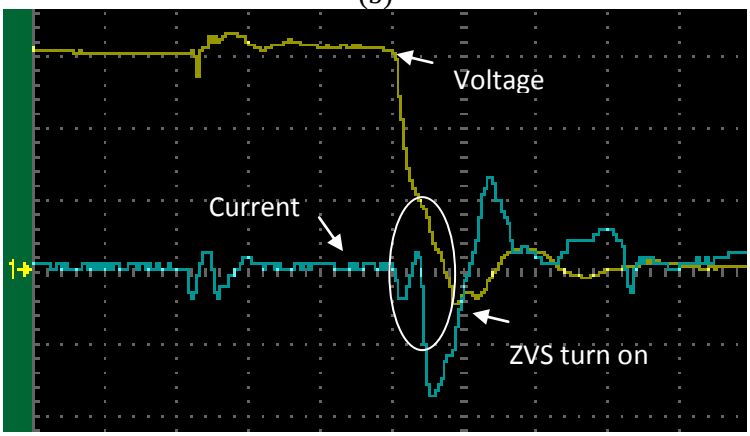

(c)

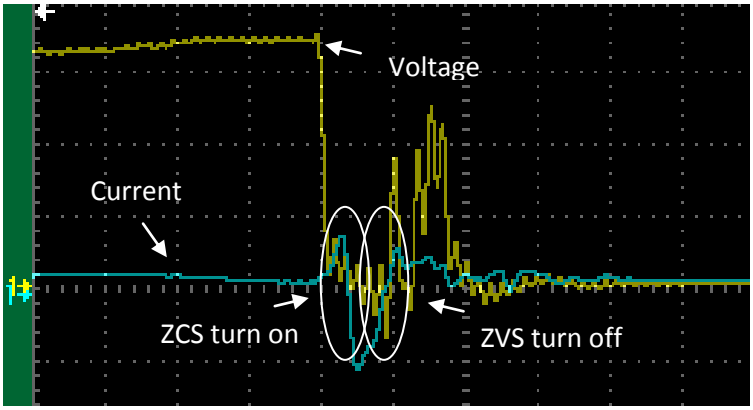

(d)

Fig.4.3 (a) Input and Output voltages(Y-axis: 10V/div, X-axis (b) Gate pulses given to main switch and auxiliary switch (c) Voltage and Current across Main switch(Y-axis: voltage=15V/div, current=500mA/div) (d) Voltage and Current across Auxiliary Switch (Y-axis: voltage=15V/div, current=500mA/div)

During turn off, the principle remains the same as the main switch as the ZVS condition is satisfied due to the anti-parallel diode. The main inductor current is shown in Fig. 4.3(e)

The efficiency of the boost converter can be studied by the fact that, in any boost converter, the maximum loss is due to the switching and conduction loss across the switches and the diodes. Hence, here these losses are considered to have a comparative analysis between the hard switching and the soft switching boost converters. The maximum efficiency is witnessed at the same power output with efficiency of around 89% for conventional hard switching converter and around 94% for the soft switching converter which is illustrated in Fig. 4.4.

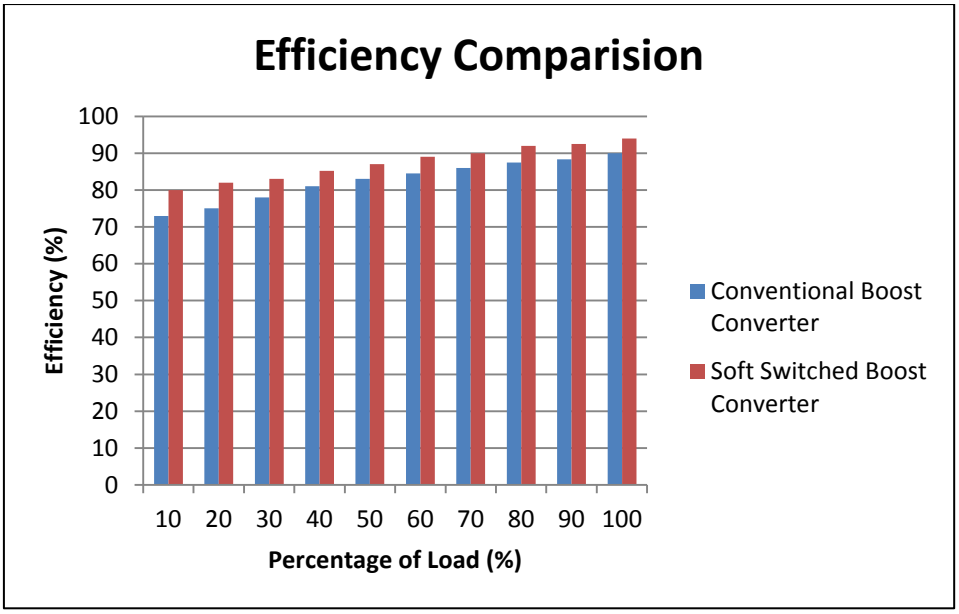

Fig. 4.4. Efficiency v/s Percentage of Load Curves

CHAPTER 5

Conclusions

5.1 CONCLUSIONS

A soft switching boost converter using an auxiliary resonant circuit employing a single diode equivalent circuit of a PV panel has been presented in this report. A new approach to mathematical modeling of PV Module is incorporated for simplicity, ease to work and fast response time for simulation purpose. For extracting maximum power from the module, Perturb and Observe (P&O) control algorithm is implemented to track the Maximum Power Point (MPP). The simulation and the experimental results verify the soft switching of both the switches. A detailed analysis of the switching losses and conduction losses of the switches and the diodes has been accomplished. A considerable difference has been found in the efficiency of the hard switching and the soft switching converter. An effective design of the inductors used in the soft switching boost converter has also been included. This soft switching technique can be used in telecom services where there is a necessity of low DC power with high DC bus voltage. Using this, it will not only result in better symbiotic working conditions and a new area of exploration: but the use of soft switching in extraction of the DC power will enhance the efficiency of the PV system implemented, thus makes the overall system cost effective.

References

[1] B.Chitti Babu, S.R.Samantaray, M.V.Ashwin Kumar, "Design and Implementation of Low Power Smart PV Energy System for Portable Applications Using Synchronous Buck Converter", *Journal of Low Power Electronics*, American Scientific publishers, Vol.08, Issue.02, pp.: 1-10, 2012.

[2] Jee-Hoon Jung, and S. Ahmed, "Model Construction of Single Crystalline Photovoltaic Panels for Real-time Simulation," IEEE Energy Conversion Congress & Expo, September 12-16, 2010, Atlanta, USA.

[3] K..N. Hasan.; et al. "An improved maximum power point tracking technique for the photovoltaic module with current mode control" In: Proc. of 19th Australian university power engineering conference (AUPEC), pp. 1-6, 2009.

[4] T.Esram, P.L. Chapman, "Comparison of Photovoltaic Array Maximum Power Point Tracking Techniques," IEEE Transactions on Energy Conversion., vol.22, no.2, pp. 439–449, June, 2007.

[5] J.Santos, F. Antunes, A. Chehab and C. Cruz, "A maximum power point tracker for PV systems using a high performance boost converter," Solar Energy, vol. 80, pp. 772-778, 2006.

[6] N. Jain,"A Zero Voltage Switching Boost Converter using a Soft Switching Auxiliary Circuit with reduced conduction losses", M.S.Thesis, Concordia University, Montreal, Canada. December 2000.

[7] S.Wang, "Design and hardware implementation of a soft-switched converter for fuel cell applications", M.S.Thesis, University of Texas, Arlington. May 2006.

[8] MiroslawLuft, ElzbietaSzychta and LeszekSzychta, "Method of designing ZVS boost converter," *Power Electronics and Motion Control Conference 2008*(EPEPEMC 2008), Poznan(Poland), September 2008.

[9] HacyBodur and A. FarukBakan, "A new ZVT-PWM DCDC converter," *IEEE Trans. on Power Electronics*, vol. 17, no. 1, pp. 40-47, January 2002.

[10] R. Gurunathan and A. K. S. Bhat, "A zero-voltage transition boost converter using a zero-voltage switching auxiliary circuit," *IEEE Trans. on Power Electronics*, vol. 17, no. 5, pp. 658-668, September 2002.

[11] Prasanna, U.; Rathore, A.; , "Extended Range ZVS Active-Clamped Current-Fed Full-Bridge Isolated Dc/Dc Converter for Fuel Cell Applications: Analysis, Design and

Experimental Results," *IEEE Transactions on Industrial Electronics*, , Vol. 59,No:12., pp.1, 2012.

[12] E..H. Kim and B.H. Kwon, "Zero-voltage- and zero current-switching full-bridge converter with secondary resonance," IEEE Trans. On Industrial Electronics, vol. 57, no. 3, pp. 1017-1025, March 2010.

[13] S.H. Park, G.R. Cha, Y.C. Jung and C.Y. Won, "Design and application for PV generation system using a soft switching boost converter with SARC," IEEE Trans. on Industrial Electronics, vol. 57, no. 2, pp515-522, February (2010).

APPENDIX

A.1 MPP TRACKING USING PERTURB AND OBSERVE METHOD

A PV panel requires a tracker to track the maximum power point (MPP) at all-time irrespective of the alterations in temperature and irradiation and the corresponding flow chart for implementing P&O method is shown in fig.4. A tracker consists of: a switch-mode boost converter to provide constant output voltage and a control with tracking capability to provide fixed input voltage to hold the array at maximum power point. Perturb and Observe (P&O) method periodically increments or decrements the panel voltage and compares the PV output power with that of the previous cycle. If the perturbation leads to an increase/decrease in module power, the subsequent perturbation occurs in the same/opposite direction. However, it has two parameters: the step size and the time between algorithm iteration. Hence, for faster tracking with accuracy, a trade-off is made between the two parameters.

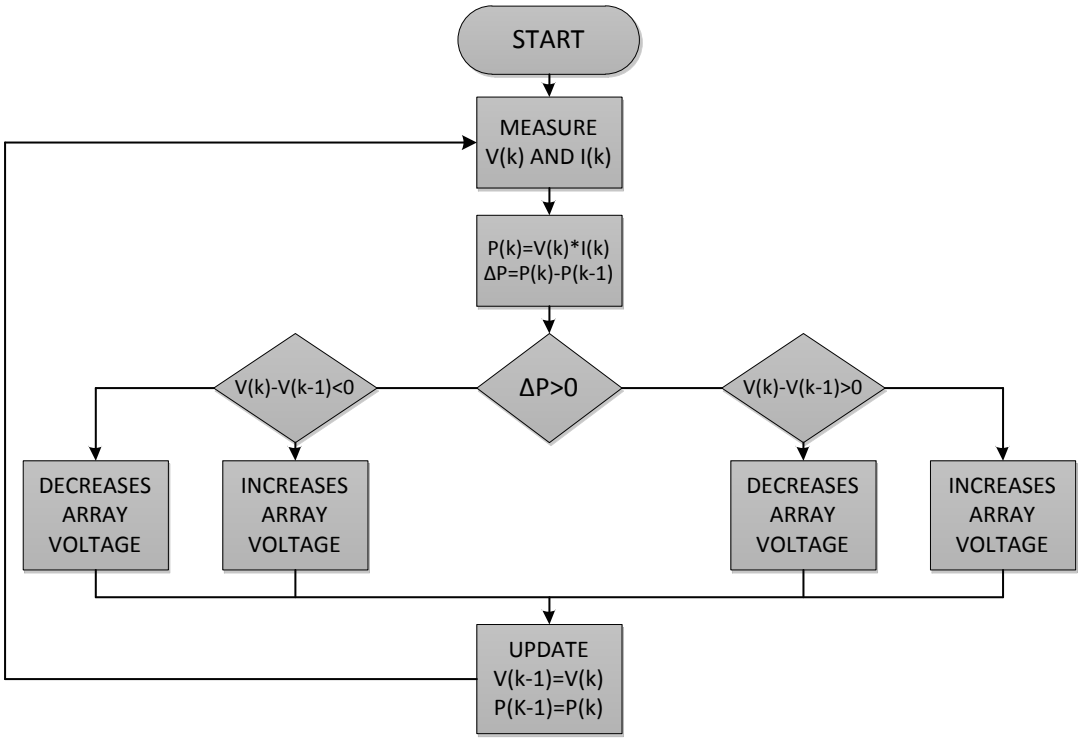

Fig.A.1. Flowchart for Perturb and Observe Method

A.2 Loss Calculation at different modes

Modes	*Conduction Losses (in mW)*						*Switching Losses(in mW)*
	S_a	**S_m**	**D_a**	**D_{out}**	**D_{Sm}**	**D_{Sa}**	**D_a**
Mode 1	1.08			1.512			
Mode 2	5.39						
Mode 3	0.2246				0.546		
Mode 4	0.0163	1.97					
Mode 5		0.020				0.0204	
Mode 6		0.755					0.6790
Mode 7			4.284				
Mode 8			3.024	4.032			
Mode 9				0.143			0.10125

A.3 Parameters of the PV Array

Parameters	*Value*
P_{MAX}	36 W
V_{MAX}	17V
I_{MAX}	2.17A
V_{OC}	21.0V
I_{SC}	2.35A

PAPERS PUBLISHED

1. **Satarupa Bal**, B.Chitti Babu, Anup Anurag" An improved Soft Switching DC-DC Converter for low power PV applications", *Journal of Low Power Electronics*, American Scientific publishers- ***Accepted for Special Issue***, *Vol.09, No:3, Oct 2013.*
2. **Satarupa Bal**, Anup Anurag, B.Chitti Babu," Comparative Analysis of Mathematical Modelling of Photo-Voltaic (PV) Array", In Proc. IEEE INDICON International Conference 2012, Dec/2012.
3. **Satarupa Bal**, Anup Anurag, B.Chitti Babu," An improved Soft Switching DC-DC Converter for low power PV applications", In Proc. 3rd IEEE International Symposium on Electronic System Design" (ISED 2012), Dec/2012, BESU, Shibpur.